

Theoretical Studies of Excitation in Low-Energy Electron-Polyatomic Molecule Collisions

*T.N. Rescigno, C.W. McCurdy, W.A. Isaacs, A.E. Orel,
H.-D. Meyer*

This article was submitted to
22nd International Conference on Photonic, Electronic and Atomic
Collisions, Santa Fe, New Mexico, July 18-24, 2001

U.S. Department of Energy

Lawrence
Livermore
National
Laboratory

August 13, 2001

DISCLAIMER

This document was prepared as an account of work sponsored by an agency of the United States Government. Neither the United States Government nor the University of California nor any of their employees, makes any warranty, express or implied, or assumes any legal liability or responsibility for the accuracy, completeness, or usefulness of any information, apparatus, product, or process disclosed, or represents that its use would not infringe privately owned rights. Reference herein to any specific commercial product, process, or service by trade name, trademark, manufacturer, or otherwise, does not necessarily constitute or imply its endorsement, recommendation, or favoring by the United States Government or the University of California. The views and opinions of authors expressed herein do not necessarily state or reflect those of the United States Government or the University of California, and shall not be used for advertising or product endorsement purposes.

This is a preprint of a paper intended for publication in a journal or proceedings. Since changes may be made before publication, this preprint is made available with the understanding that it will not be cited or reproduced without the permission of the author.

This report has been reproduced directly from the best available copy.

Available electronically at <http://www.doe.gov/bridge>

Available for a processing fee to U.S. Department of Energy
and its contractors in paper from
U.S. Department of Energy
Office of Scientific and Technical Information
P.O. Box 62
Oak Ridge, TN 37831-0062
Telephone: (865) 576-8401
Facsimile: (865) 576-5728
E-mail: reports@adonis.osti.gov

Available for the sale to the public from
U.S. Department of Commerce
National Technical Information Service
5285 Port Royal Road
Springfield, VA 22161
Telephone: (800) 553-6847
Facsimile: (703) 605-6900
E-mail: orders@ntis.fedworld.gov
Online ordering: <http://www.ntis.gov/ordering.htm>

OR

Lawrence Livermore National Laboratory
Technical Information Department's Digital Library
<http://www.llnl.gov/tid/Library.html>

THEORETICAL STUDIES OF EXCITATION IN LOW-ENERGY ELECTRON-POLYATOMIC MOLECULE COLLISIONS

T. N. RESCIGNO^{1,2}

C. W. MCCURDY^{1,3}, W. A. ISAACS², A. E. OREL³, H. -D. MEYER⁴

¹Lawrence Berkeley National Laboratory, 1 Cyclotron Rd., Berkeley, CA 94720, USA

²Lawrence Livermore National Laboratory, PO Box 808, Livermore, CA 94551, USA

³Department of Applied Science, University of California, Davis, Livermore, CA 94551, USA

⁴Universitat Heidelberg, Im Neuenheimer Feld 229, D-69120 Heidelberg, Germany

E-mail: tnr@llnl.gov

This paper focuses on the channeling of energy from electronic to nuclear degrees of freedom in electron-polyatomic molecule collisions. We examine the feasibility of attacking the full scattering problem, both the fixed-nuclei electronic problem and the post-collision nuclear dynamics, entirely from first principles. The electron-CO₂ system is presented as an example. We study resonant vibrational excitation, showing how *ab initio*, fixed-nuclei electronic cross sections can provide the necessary input for a multi-dimensional treatment of the nuclear vibrational dynamics.

1 Introduction

For almost two decades, starting in the late 1970's, much of the *ab initio* theory on electron-molecule collisions was concerned with the technical problem of developing robust methods for solving the fixed-nuclei problem posed by electron scattering from a non-spherical, polarizable, charge distribution with full allowance for exchange. We should say at the outset that by *ab initio* methods we mean those which treat the electronic Schrödinger equation as a *many-electron* equation describing the motion of N+1 indistinguishable particles. This is not meant to diminish in any way the contribution of those who have pursued model potential approaches in which the effects of target polarization are represented by a local potential. While such approaches have proved successful in a number of cases, they are nevertheless *ad hoc* in character in the sense that they cannot be systematically improved and they are intrinsically limited in the types of collision phenomena that they can treat (electronically elastic processes, in general). Of the many approaches that have been attempted, only a few have withstood the test of time and proved robust enough to be applicable in general multi-electronic-state expansions on polyatomic targets. Significantly, the *ab initio* methods that have survived - R-Matrix, multi-channel Schwinger and complex Kohn - are all variational in nature and make use of algebraic expansions of the fixed-nuclei wave function rather than direct numerical solution of the electronic Schrödinger equation.

While the bulk of *ab initio* computational work on electron-polyatomic collisions has tended to focus on the fixed-nuclei electronic problem, it is important to bear in mind that the nuclear dynamics problem, i.e. the processes that control the flow of electronic energy into nuclear degrees of freedom, are of fundamental importance in studying electron collisions with polyatomic targets and are key to developing an understanding of *electron-driven chemistries* in a variety of contexts, from technological applications such as understanding the production of reactive species in low-temperature processing plasmas to elucidating the behavior of secondary electrons produced by low-dose radiation in biological environments.

In discussing the nuclear dynamics problem, it is useful to distinguish between resonant

and non-resonant collisions. The non-resonant dynamics problem for polyatomic targets presents some formidable challenges. For example, non-resonant electron-impact dissociation of a polyatomic can involve many excited electronic states. Tracking the dynamics on multiple electronic surfaces, where the reactive fragments can be produced with several eV of energy, is a daunting task. This problem remains largely unexplored. For resonant electron-molecule collisions, on the other hand, there has been a fair amount of theoretical work, but it has been largely semi-empirical in nature, relying on model potentials to carry out the nuclear dynamics. Moreover, with a few notable exceptions^{1,2,3}, most of the work that has been carried out, both *ab initio* and semi-empirical, has made use of one-dimensional models of the nuclear motion that is only appropriate for diatomic targets. The question we wish to explore here is whether it is feasible to treat a resonant electron-polyatomic problem in its entirety - both electronic and nuclear - from first principles. The problem we have chosen to illustrate the discussion is $e^- + \text{CO}_2$ scattering, a system which has been studied for many years and one which continues to attract the attention of both theorists and experimentalists.

While the first experiments on $e^- + \text{CO}_2$ collisions date back to 1927 with the work of Ramsauer, the computational history on this system really began with the pioneering work of Morrison, Collins and Lane in 1977⁴, who used model local potentials to reproduce the two main features seen in the measured low-energy cross sections, namely, the dramatic rise in the elastic cross section below 2 eV and the pronounced resonance structure centered at 3.8 eV. While numerous model studies have been carried out on this system over the past two decades, the first *ab initio* study to conclusively show that the low-energy rise in the elastic cross section was the result of a virtual state was carried out by Morgan in 1998⁵ using the R-matrix method. The multi-channel Schwinger calculations of Lee *et al.*⁶ and the complex Kohn calculations of Rescigno *et al.*⁷ were the first *ab initio* studies to achieve quantitative agreement with experiment on both the low-energy behavior of the total cross section and the position of the resonance peak; the latter study also obtained differential cross sections in good accord with recent measurements^{8,9}. Our purpose here is to examine the structure of the resonant vibrational excitation cross sections in more detail using an entirely *ab initio* attack on the problem.

2 Fixed-Nuclei Electronic Problem

2.1 Complex Kohn Method

Our approach to low-energy electron-polyatomic molecule scattering is based on the complex Kohn variational method, which uses a stationary principle for the T-matrix:

$$T_{stat}^{\Gamma\Gamma_0} = T_{trial}^{\Gamma\Gamma_0} - 2 \int \Psi_{\Gamma}(H - E)\Psi_{\Gamma_0}. \quad (1)$$

The trial wave function for the $(N + 1)$ -electron system is expanded as

$$\Psi_{\Gamma_0} = \sum_{\Gamma} A[\Phi_{\Gamma}(\vec{r}_1 \dots \vec{r}_N) F_{\Gamma\Gamma_0}(\vec{r}_{N+1})] + \sum_{\mu} d_{\mu}^{\Gamma_0} \Theta_{\mu}(\vec{r}_1 \dots \vec{r}_{N+1}) \quad (2)$$

where the first sum is over electronic target states, Φ_{Γ} , A antisymmetrizes the coordinates of the incident electron with those of the target electrons and the second sum contains square-integrable, $(N + 1)$ -electron terms that describe correlation and polarization effects.

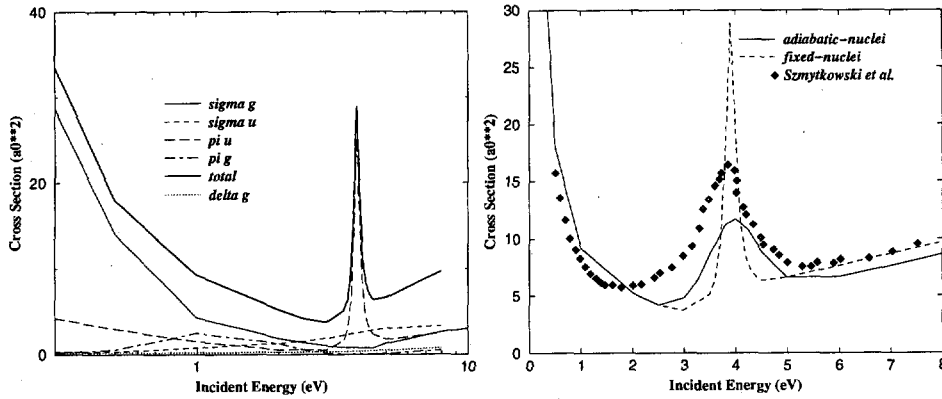


Figure 1. Left panel: fixed-nuclei integrated cross sections for $e^- + \text{CO}_2$ at equilibrium geometry. Right panel: Comparison of fixed-nuclei, adiabatic-nuclei and measured total cross sections for $e^- + \text{CO}_2$ ¹¹.

In the Kohn method, the scattering functions are further expanded in a combined basis of Gaussian(ϕ) and continuum(Ricatti-Bessel, j_l , and Hankel, h_l^+) basis functions:

$$F_{\Gamma\Gamma_o}(\vec{r}) = \sum_i c_i^{\Gamma\Gamma_o} \phi_i(\vec{r}) + \sum_{lm} [j_l(k_{\Gamma}r) \delta_{l_0} \delta_{mm_0} + T_{l_0mm_0}^{\Gamma\Gamma_o} h_l^+(k_{\Gamma}r)] Y_{lm}(\vec{r})/r. \quad (3)$$

The T-matrix elements, $T_{l_0mm_0}^{\Gamma\Gamma_o}$, are the fundamental dynamical quantities from which all fixed-nuclei cross sections are derived.

For the calculations on CO_2 , we have restricted our attention to the electronically elastic region, so the sum over target states in Eq. (2) includes only the ground state and we can drop the $\Gamma\Gamma_o$ superscript on the T-matrix elements. For the ground state of CO_2 , we employed a self-consistent field (SCF), restricted Hartree-Fock wave function. To describe the dynamic polarization of the target, we also include $(N + 1)$ -electron terms in the trial function that represent asymptotically decaying closed channels. These terms are chosen by singly exciting the occupied target orbitals into unoccupied virtual orbitals. The procedures used for this construction vary according to the symmetry under consideration. For the symmetries in which there are no low-lying shape resonance, i.e. all but ${}^2\Pi_u$, we construct "polarized-orbitals" for the virtual space, single excitations into which give a good representation of the static target polarizability. For the resonance symmetry, we use a "relaxed-SCF" procedure which only includes symmetry- and spin-conserving single excitations of the target, thereby capturing the dominant physical effect of a shape resonance which is relaxation of the target in the presence of an extra electron. These procedures, along with other parameters of the calculations, are fully described in ref. 7.

Figure 1 shows the fixed-nuclei total cross sections, along with the values for the individual symmetry components, that were computed at the equilibrium geometry of the target, i.e. linear geometry with a CO bond distance of 2.1944 bohr. These results highlight the two main features of the cross sections previously mentioned. The dramatic rise in the cross section below 2 eV is clearly associated with the ${}^2\Sigma_g^+$ component of the total cross section while the resonance feature near 4 eV is associated with the ${}^2\Pi_u$ component.

2.2 Adiabatic Nuclei Approximation

The preponderance of electron-molecule calculations reported in the literature were performed at the equilibrium geometry of the nuclei. These cross sections correspond, in general, to rotationally and vibrationally summed quantities in cases where the internal target motion of the nuclei can be neglected. These assumptions frequently break down in resonance regions. The fixed-nuclei results shown in Fig. 1, when compared to experiment, produce a resonance feature whose peak value is too high and whose width is too broad. This deficiency arises from a neglect of vibrational motion.

The adiabatic nuclei approximation represents a first step in accounting for nuclear motion. One assumes the Born-Oppenheimer approximation to be valid for the scattering states and writes them as products of electronic continuum functions times target vibrational functions. If one further ignores the dependence of the free electron wave vector on the target vibrational state, then the body-frame T matrix can be written:

$$\langle k_{\nu'} \nu' | T | k_{\nu} \nu \rangle \approx \sum_{l' m m'} i^{l-l'} Y_{lm}(\hat{k}) Y_{l'm'}^*(\hat{k}') \int ds \eta_{\nu'}(s) T_{ll' m m'}^k(s) \eta_{\nu}(s), \quad (4)$$

where the vibrational functions are η_{ν} and $\eta_{\nu'}$ and the variable s is used to denote the internal vibrational coordinates. Thus the adiabatic nuclei approximation for vibrational excitation cross sections requires integrals of the individual fixed-nuclei T-matrix elements, which depend parametrically on internal target geometry, between the target vibrational wave functions. If we are not interested in the individual vibrational levels, then we can sum Eq. 4 over the final ν' levels, using the completeness relation

$$\sum_{\nu'} \eta_{\nu'}(s) \eta_{\nu}(s) = \delta(s - s'), \quad (5)$$

to obtain the following expression for the total cross section:

$$\sigma^{total} = \int ds \eta_{\nu}^2(s) \sigma(s). \quad (6)$$

In our earlier work on this system ⁷, we used the adiabatic nuclei treatment outlined above to examine the importance of nuclear motion on the total cross section, considering only the effect of the symmetric-stretch mode. Cadez *et al.* ¹⁰ had noted that the resonance couples most strongly to symmetric-stretch motion, having observed energy-loss spectra at 4 eV for pure symmetric-stretch up to $\eta_{\nu'}=25$. The right panel of Fig. 1 shows both the fixed-nuclei and adiabatic nuclei results for the total integrated cross section, along with measured values. The effect of nuclear motion is clearly to broaden and lower the resonance feature, bringing the results into better agreement with experiment. ¹¹ It is also clear from this comparison that a more sophisticated treatment of nuclear motion is needed to quantitatively describe the cross section in the resonance region.

3 Formal Resonance Theory

3.1 Time-independent Formulation

Computational treatments of resonant vibrational excitation are generally based on rigorous resonance scattering theory ¹², formulated within the Born-Oppenheimer approximation.

The principle result of the theory is the so-called nuclear wave equation that governs the nuclear dynamics due to the resonance state(s):

$$[E - E_{res} - K_s]\xi_{\nu_i}(s) = (\psi_{res}H_{el}P\phi_{\nu_i}) + (\psi_{res}H_{el}PG_P^+PH_{el}\psi_{res})\xi_{\nu_i}(s), \quad (7)$$

where K_s is the nuclear kinetic energy operator, H_{el} is the fixed-nuclei electronic Hamiltonian, ψ_{res} is the electronic resonance wave function and P projects onto the non-resonant background. This is an inhomogeneous wave equation which, due to the presence of the nuclear Greens's function, G_P^+ , involves an effective Hamiltonian that is complex, non-local and energy dependent. Rather than deal directly with this equation, we use the simpler "boomerang" or local complex potential model:¹³

$$(E - K_s - E_{res}(s) + i\Gamma(s)/2)\xi_{\nu}(s) = \phi_{\nu}, \quad (8)$$

which can be derived by starting with Eq. 7 and making several simplifying approximations. The conditions under which these approximations are valid have been well documented¹⁴. In Eq. (8), $E_{res}(s)$ and $\Gamma(s)$ are the position (real part) and width (imaginary part) of the resonance energy surface, respectively and the 'entry amplitude', ϕ_{ν} , is defined as:

$$\phi_{\nu}(s) = (\Gamma(s)/2\pi)^{1/2}\eta_{\nu} \quad (9)$$

The resonant T-matrix for vibrational excitation is obtained by projecting the solution of Eq. (8) onto the 'exit amplitude', $\phi_{\nu'}$:

$$T_{\nu\nu'}(E) = \langle \phi_{\nu'} | \xi_{\nu} \rangle. \quad (10)$$

Eq. (10) can equivalently be written as the matrix element of a nuclear Green's function between entry and exit amplitudes:

$$T_{\nu\nu'}(E) = \langle \phi_{\nu'} | \frac{1}{E - K_s - E_{res}(s) + i\Gamma(s)/2} | \phi_{\nu} \rangle \quad (11)$$

3.2 Time-dependent Formulation

The differential equations of the boomerang model may be recast in a time-dependent formulation, as first shown by McCurdy and Turner¹⁵, by writing the nuclear Green's function as the Fourier transform of the propagator for the time-dependent Schrödinger equation. The resonant T-matrix for vibrational excitation is then expressed as:

$$T_{\nu\nu'}(E) = -i \int_0^{\infty} dt e^{iEt} \langle \phi_{\nu'} | \Psi_t \rangle \quad (12)$$

with

$$\Psi_t = e^{-iHt}\phi_{\nu} \quad (13)$$

and

$$H = K_s + E_{res}(s) - i\Gamma(s)/2 \quad (14)$$

The meaning of Eqs. (12-14) is clear: the resonant transition amplitude for excitation is given as the Fourier transform of the overlap between a wave packet propagating on a complex potential surface and a stationary packet determined by the final state. Since the potential surface is complex, the wave packet normalization is not conserved and the packet

decays exponentially as a function of time at a rate determined by the magnitude of the resonance width.

For problems with only one nuclear degree of freedom, there are no obvious computational advantages in choosing the time-dependent approach over the time-independent approach other than for the physical insight it offers into the problem. However, for problems with multiple degrees of freedom, there are decided advantages to the time-dependent approach, since it does not involve the solution of large systems of complex linear equations and it can be made quite efficient, as we shall see.

3.3 Solving the Time-dependent Schrödinger Equation

The "standard" method for solving the time-dependent Schrödinger equation proceeds by introducing a discrete set of points for each degree of freedom and constructing an explicit solution of the first-order linear equations that represent the equations of motion for a wave packet propagating in time on the discrete grid. A variety of computational methods are available for approximating the propagator. The problem with the standard method is that the computational effort required scales exponentially with the number of degrees of freedom, making it prohibitively expensive to implement as the number of degrees of freedom grows.

To remove this obstacle, approximate methods have been developed. In the time-dependent Hartree (TDH) method, for example, the wave function is represented as a single product of one-dimensional functions, thereby simplifying the computational effort at the cost of a proper treatment of correlation between the degrees of freedom. The multi-configuration time-dependent Hartree (MCTDH) method¹⁶ offers a practical alternative to the TDH method that retains the essential rigor of the standard method. In the MCTDH method, as in the standard method, we start with a time-independent orthonormal product basis set:

$$\{\chi_{j_1}^{(1)}(Q_1) \dots \chi_{j_f}^{(f)}(Q_f)\}, \quad j_i = 1..N_i \quad (15)$$

where we have assumed that there are f degrees of freedom in a problem described by nuclear coordinates Q_1, \dots, Q_f . For computational efficiency, the basis functions, $\chi_{j_i}^{(i)}$, are chosen as the basis functions of a discrete variable representation (DVR)¹⁷.

The central idea in the MCTDH scheme is that one can employ a smaller, but now time-dependent, basis for expanding the wave function, i.e.

$$\Psi(Q_1, \dots, Q_f, t) = \sum_{j_1=1}^{n_1} \dots \sum_{j_f=1}^{n_f} A_{j_1 \dots j_f}(t) \prod_{k=1}^f \varphi_{j_k}^{(k)}(Q_k, t), \quad (16)$$

with $n_k \ll N_k$. The single-particle functions in turn are represented as linear combinations of the primitive basis

$$\varphi_{j_k}^{(k)}(Q_k, t) = \sum_{i_k=1}^{N_k} c_{i_k j_k}^{(k)}(t) \chi_{i_k}^{(k)}(Q_k) \quad (17)$$

Since both the coefficients, $A_{j_1 \dots j_f}$, and the single-particle functions are time-dependent, the wave function representation is not unique. Uniqueness can be achieved by imposing

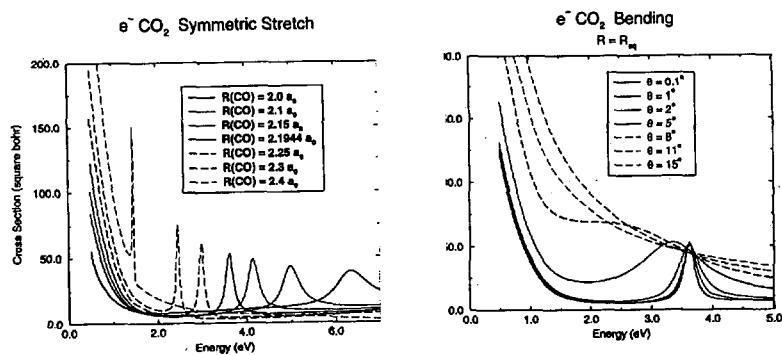


Figure 2. $e^- + \text{CO}_2$ fixed-nuclei integrated cross sections in 2A_1 symmetry. Left panel: symmetric-stretch dependence in linear geometry. Right panel: bend-angle dependence at equilibrium CO bond distance.

additional constraints on the single-particle functions which keep them orthonormal for all times¹⁶.

In our calculations on CO_2 , we have tested the accuracy of the MCTDH scheme by carrying out boomerang calculations in both 1D and 2D using both the standard method and MCTDH method. The two methods produced virtually identical results for this problem. For the 3D calculations, we used only the MCTDH method.

4 Computational Results for CO_2

4.1 Electronic Resonance Energy Surface

To recapitulate briefly, we first carry out fixed-nuclei scattering calculations, using the complex Kohn method, at a number of different nuclear geometries. To date, we have considered both symmetric-stretch and bending geometries. From these calculations, we obtain a resonance energy and width at each geometry from a Breit-Wigner fit of the electronic scattering data. This data defines a complex potential energy surface on which the time-dependent wave packet dynamics calculations are carried out. We also use the computed potential energy surface of the neutral CO_2 molecule to compute the initial and final target vibrational wave functions. Fig. 2 gives a representative sampling of the fixed-nuclei ${}^2\Pi_u({}^2A_1)$ cross sections for linear(bent) geometries. The left panel of the figure shows that, as the molecule is stretched from its equilibrium position, the resonance energy drops and the width decreases. The right panel shows that bending the molecule causes the resonance to broaden dramatically as it decreases in energy. From results such as these, we are able to construct the resonance energy and width surfaces shown in Figure 3.

One notes that the resonance width goes to zero as the molecule is either stretched or bent sufficiently, reflecting the known fact^{18,19} that the 2A_1 state of CO_2^- becomes a stable negative ion, i.e. is electronically bound, at such geometries. The topology of the width surface shows that for OO bond distances less than 5 bohr, bending the molecule causes the resonance width to increase sharply before it eventually turns over at larger angles. This behavior will be seen to have a significant effect on the vibrational excitation cross sections.

There are several points to be made when considering these results. Symmetric-stretch

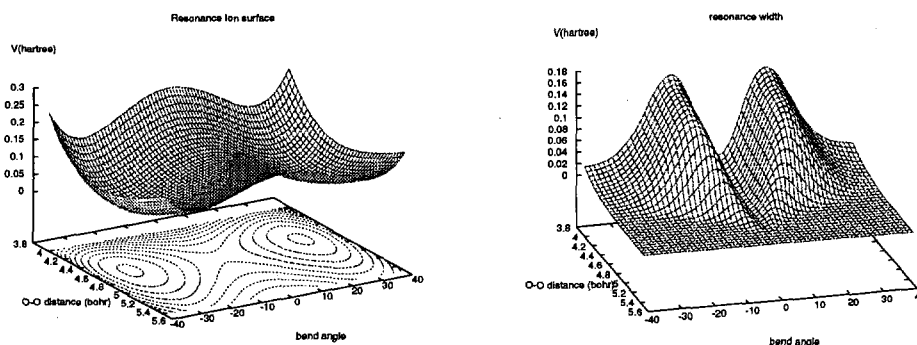


Figure 3. Complex 2A_1 resonance energy of CO_2^- a function of symmetric-stretch distance and bend angle. Left panel shows the real part of the energy surface and the right panel shows the corresponding width.

motion with zero bend angle does not change the symmetry of the molecule and hence does not significantly change the angular momentum character of the resonance, whose lowest l component at equilibrium is p -wave. Bending the molecule, however, breaks the degeneracy of the ${}^2\Pi_u$ resonance and mixes an s -wave component into the 2A_1 resonance. There is no angular momentum barrier associated with an s -wave so it is not surprising that such an admixture causes the lifetime of the resonance to decrease. It should also be noted that bending causes the initially degenerate ${}^2\Pi_u$ resonance to split into 2A_1 and 2B_1 components and that in these initial calculations we have only considered the 2A_1 resonance state.

4.2 One-dimensional Boomerang Results

We first computed cross sections for symmetric-stretch excitation using a one-dimensional boomerang treatment that constrained the nuclei to lie along a line. Cadez *et al.*¹⁰ had previously carried out such calculations, using semi-empirically determined resonance parameters chosen to give a best fit to their measured cross sections. Figure 4 shows our 1D results for the resonant elastic and $0 \rightarrow 1$ vibrational excitation cross sections. The results at this level give something of a textbook picture of a 'diatomic' shape resonance, similar to what is found in N_2 , with deep, well-defined interference structures¹³. Experiment^{10,20}, however, shows structure that is far less pronounced than what these 1D results predict, with very shallow valleys between adjacent peaks. That Cadez *et al.*¹⁰ were able to produce so little structure with their model calculations can be understood by comparing their empirically determined resonance parameters with our calculated results. While the real part of the resonance curve they derived is very close to our *ab initio* result (as is should be, since this parameter determines the position and overall envelope of the cross section), the width function they derived is significantly larger than our results in the critical regions that the wave packet samples. This comparison serves to highlight the limitations of a 1D treatment and provided much of the impetus for the multi-dimensional studies we undertook.

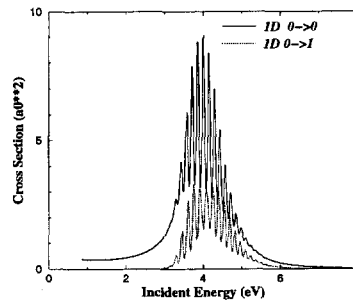


Figure 4. One-dimensional (symmetric-stretch) boomerang results for e-CO₂ elastic (0 → 0) and vibrationally inelastic (0 → 1) cross sections.

4.3 Multi-dimensional Results

The multi-dimensional wave packet calculations were carried out using normal coordinates, with the restriction that the two CO bond distances were restricted to be the same. The symmetric-stretch coordinate, S_1 , and the doubly degenerate bend coordinates, S_{2a} and S_{2b} , are defined as:

$$S_1 = 2R \cos \theta \quad (18)$$

$$S_{2a}^2 + S_{2b}^2 = R^2 \sin^2 \theta / (1 + m_C / (2m_O))^2 \quad (19)$$

The vibrational wave functions of the neutral target were approximated as uncoupled products of normal coordinate wave functions. We carried out MCTDH calculations in both two- and three-dimensions. The 2D calculations restrict the nuclei to move in a fixed plane by considering only one of the two degenerate bending modes. Figure 5 shows results for the vibrationally elastic cross sections. The left panel compares the resonant elastic cross sections computed in 1D, 2D and 3D, and shows that the pronounced interference features seen in the 1D calculations are strongly damped in 2D since the wave packet decays rapidly as it samples the non-linear regions of the resonance surface where the width is large. The 3D calculations show no interference structure at all. To compare with experiment, we must add the non-resonant background cross section to the resonant values provided by the boomerang calculations. Those values were taken from our earlier adiabatic nuclei calculations⁷ and added to the 3D boomerang results to produce the results shown in the right panel of Fig. 5. Of the two sets of experimental data shown^{8,9}, our results are in better agreement with the results of Tanaka *et al.*⁸.

We now turn to the vibrational excitation cross sections which are shown in Fig. 6. The 0 → 1 symmetric-stretch [(0, 0, 0) → (1, 0, 0)] cross sections, computed in 1D, 2D and 3D, are shown in the left panel. While the magnitude and shape of the overall envelope of the cross section is seen to be rather insensitive to the dimensionality of the calculation, the pattern of the interference behavior is seen to follow the same trends observed in the case of the elastic cross sections. The right panel shows the 0 → 2[(0, 0, 0) → (0, 2, 0)] bending cross sections in 2D and 3D. (We note that the resonance model gives zero probability for exciting an odd number of bending quanta from the ground-state because of the symmetry of the ²A₁ resonance surface.) We again find that the 3D result shows no interference

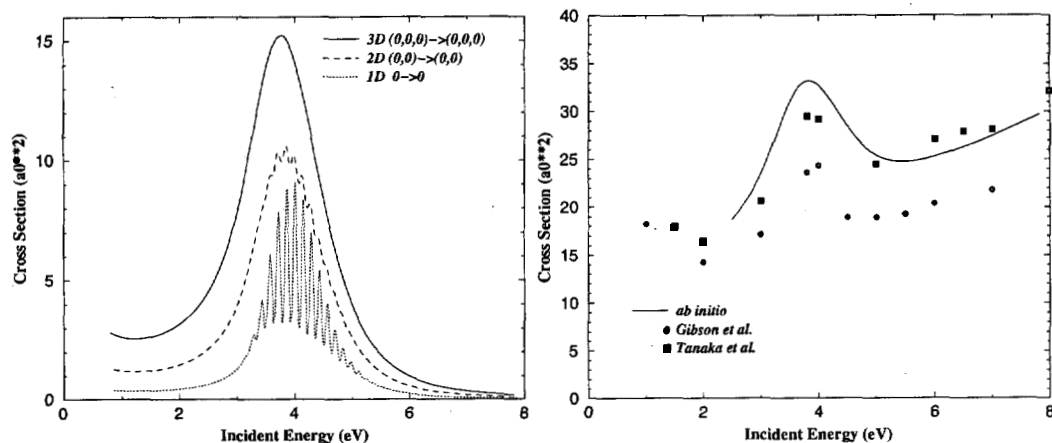


Figure 5. Integrated vibrationally elastic cross sections for $e^- + \text{CO}_2$. Left panel: resonant cross sections from 1, 2 and 3D boomerang calculations. Right panel: 3D resonant + calculated background elastic cross sections from Rescigno *et al.*⁷ compared with experimental results of Tanaka *et al.*⁸ and Gibson *et al.*⁹.

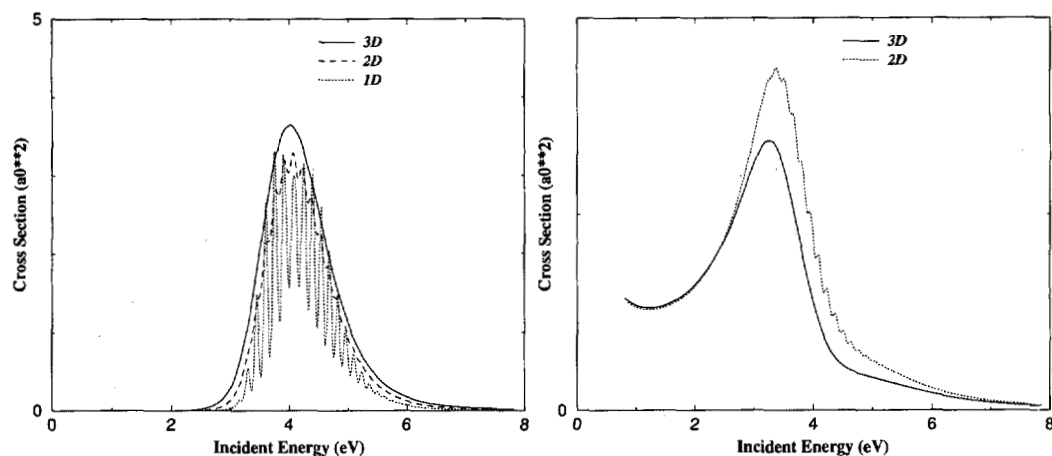


Figure 6. Integrated vibrationally inelastic cross sections for $e^- + \text{CO}_2$. Left panel: resonant symmetric-stretch $(0,0,0) \rightarrow (1,0,0)$ cross sections from 1, 2 and 3D boomerang calculations. Right panel: resonant bending $(0,0,0) \rightarrow (0,2,0)$ cross sections from 2 and 3D boomerang calculations.

structure, but there is a noticeable rise in the background cross section, in both 2D and 3D, that appears at low collision energies.

There is an accidental near degeneracy, or Fermi resonance, between the $(1,0,0)$ and $(0,2,0)$ vibrational levels of CO_2^- . For this reason, the normal mode description of the vibrational wave functions we have been using is not valid, as the true wave functions of this "Fermi dyad" are almost 50-50 mixtures of zeroth-order symmetric-stretch and bend states²¹. Therefore, to make a meaningful comparison with experiment, we must compute

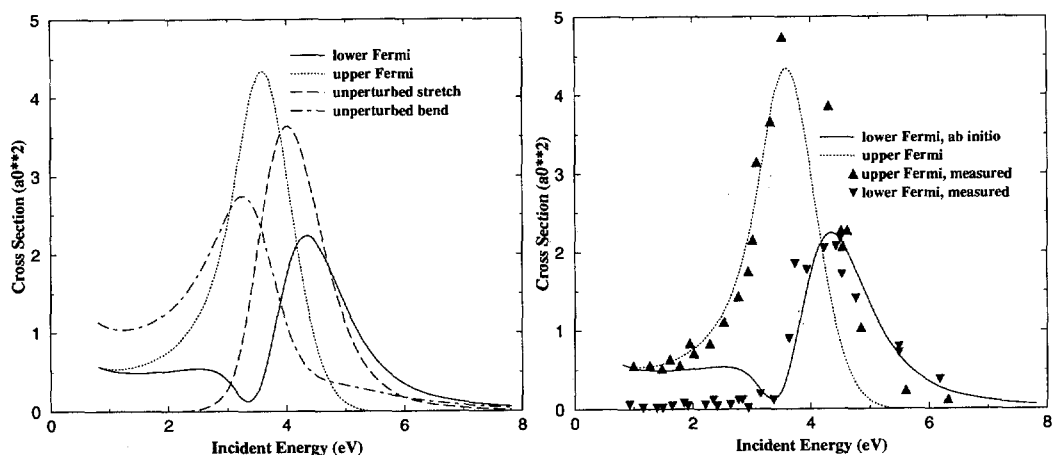


Figure 7. The effect of Fermi resonance on vibrationally inelastic cross sections for $e^- + \text{CO}_2^-$. Left panel: comparison of vibrational excitation cross sections computed using unperturbed and perturbed (Fermi dyad) representations of the vibrational wave functions. Right panel: Comparison of computed cross sections for Fermi dyad with experimental results of Johnstone *et al.*²⁰.

the cross sections from appropriate linear combinations of the computed excitation *amplitudes* that represent the proper admixture of the zeroth-order states that describe the wave functions for the two components of the dyad. These results are shown in Figure 7. The effect of the Fermi resonance on the cross sections is strikingly important, with shifts in the peak positions of $\sim .5$ eV and significant changes in the shape of the cross sections. The calculated results are also seen to be in rather good agreement with experiment²⁰. On the low energy side of the resonance profile (<3 eV), we find a nonvanishing background value for both cross sections, while experiment indicates that only the upper Fermi level has a nonzero background.

5 Discussion

Resonant electron collisions with polyatomic molecules provide an opportunity to explore a rich body of physics involving the channeling of energy into various nuclear degrees of freedom. Our calculations on the $e^- + \text{CO}_2$ system demonstrate the feasibility of approaching such a problem completely from first principles and clearly show the importance of a multi-dimensional treatment of the dynamics. While our calculations have clearly been successful in explaining much of observed experimental data, a number of issues remain to be explained.

Using decisively improved electron spectrometers with a resolution of 7 meV, Allan²² has just announced that he was able to resolve the two peaks of the CO_2 dyad and has published new values for the vibrational excitation cross sections, at a fixed angle, with very high energy resolution. His results show that there is indeed very weak interference structure of about the same scale that we found in our 2D calculations. We hasten to add that our calculations so far have only treated the 2A_1 component of the resonance.

Preliminary calculations show that the width of the 2B_1 resonance, which is degenerate with 2A_1 in linear geometry, has very little dependence on the bend angle. Therefore, we expect wave packet calculations on this other surface to show more structure. Moreover, interference effects arising from non-adiabatic coupling between the two surfaces might also account for the vanishing background cross section for the lower component of the Fermi dyad. These intriguing possibilities clearly indicate that there is more work to be done on this problem.

Acknowledgments

This work was performed under the auspices of the US DOE by the Lawrence Berkeley and Lawrence Livermore National Laboratories under contracts DE-AC03-76SF00098 and W-7405-Eng-48, respectively. The work was supported by the US DOE Office of Basic Energy Science, Division of Chemical Sciences and computations were carried out at the National Energy Research Supercomputer Center at Lawrence Berkeley National Laboratory. A.E.O. acknowledges support from the National Science Foundation (Grant No. PHY-99-87877).

References

1. A. E. Orel and K. C. Kulander, *Phys. Rev. Lett.* **71**, 4315 (1993).
2. A. K. Kazansky and L. Y. Sergeeva, *J. Phys. B* **27**, 3217 (1994).
3. A. K. Kazansky, *Opt. Spectros.* **87**, 840 (1999).
4. M. A. Morrison, N. F. Lane and L. A. Collins, *Phys. Rev. A* **15**, 2186 (1977).
5. L. A. Morgan, *Phys. Rev. Lett.* **80**, 1873 (1998).
6. C.-H. Lee, C. Winstead and V. McKoy, *J. Chem. Phys.* **111**, 5056 (1999).
7. T. N. Rescigno, D. A. Byrum, W. A. Isaacs and C. W. McCurdy, *Phys. Rev. A* **60**, 2186 (1999).
8. H. Tanaka *et al*, *Phys. Rev. A* **57**, 1798 (1998).
9. J. C. Gibson *et al*, *J. Phys. B* **32**, 213 (1999).
10. I. Cadez, F. Gresteau, M. Tronc and R. I. Hall, *J. Phys. B* **10**, 3821 (1977).
11. C. Szmytkowki *et al*, *J. Phys. B* **20**, 5817 (1987).
12. T. F. O'Malley, *Phys. Rev.* **150**, 14 (1966).
13. D. T. Birtwistle and A. Herzenberg, *J. Phys. B* **4**, 53 (1971).
14. A. U. Hazi, T.R. Rescigno and M. Kurilla, *Phys. Rev. A* **23**, 1089 (1981).
15. C. W. McCurdy and J. L. Turner, *J. Chem. Phys.* **78**, 6773 (1983).
16. M. H. Beck, A. Jackle, G. A. Worth and H.-D. Meyer, *Phys. Rep.* **324**, 1 (2000).
17. J. C. Light, "Discrete variable representations in quantum dynamics", in *Time-Dependent Quantum Molecular Dynamics*, J. Broeckhove and L. Lathouwers, Eds. (Plenum, New York, 1992).
18. D. G. Hopper, *Chem. Phys* **53**, 85 (1980).
19. G. L. Gutsev, R. J. Bartlett and R. N. Compton, *J. Chem. Phys.* **108**, 6756 (1998).
20. W. M. Johnstone, P. Akther and W. R. Newell, *J. Phys. B* **28**, 743 (1995).
21. G. Herzberg, "Molecular Spectra and Molecular Structure II. Infrared and Raman Spectra of Polyatomic Molecules", (Van Nostrand Reinhold, 1945).
22. M. Allan, *Phys. Rev. Lett.* **87**, 033201 (2001).